Heterogeneous Catalysis Hot Paper

How to cite: *Angew. Chem. Int. Ed.* **2022,** *61*, e202115100
International Edition: doi.org/10.1002/anie.202115100
German Edition: doi.org/10.1002/ange.202115100

Vectorial Catalysis in Surface-Anchored Nanometer-Sized Metal–Organic Frameworks-Based Microfluidic Devices

*Anna Lisa Semrau, Philip M. Stanley, Dominik Huber, Michael Schuster, Bauke Albada, Han Zuilhof, Mirza Cokoja, and Roland A. Fischer**

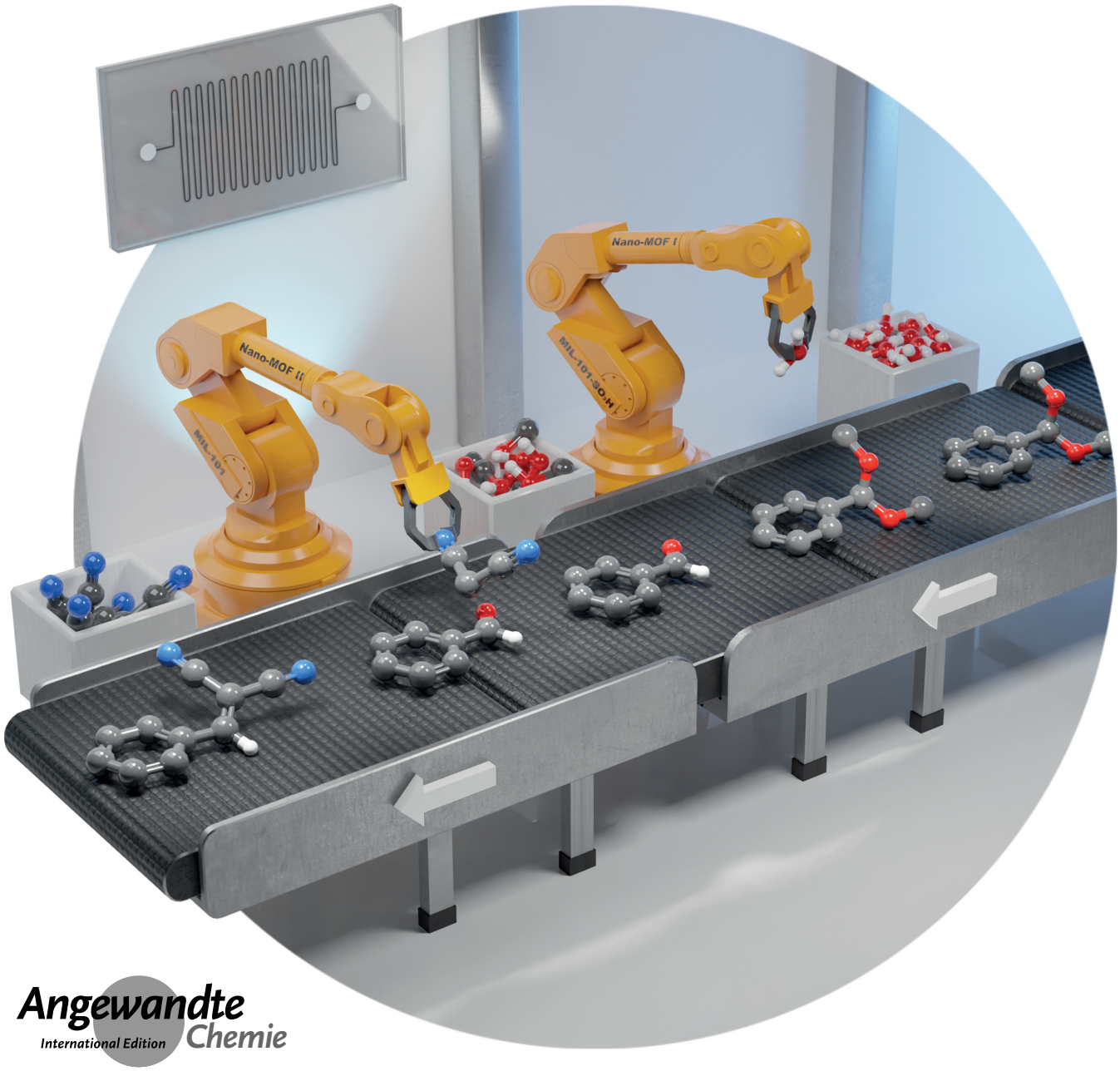

Abstract: *Vectorial catalysis—controlling multi-step reactions in a programmed sequence and by defined spatial localization in a microscale device—is an enticing goal in bio-inspired catalysis research. However, translating concepts from natural cascade biocatalysis into artificial hierarchical chemical systems remains a challenge. Herein, we demonstrate integration of two different surface-anchored nanometer-sized metal–organic frameworks (MOFs) in a microfluidic device for modelling vectorial catalysis. Catalyst immobilization at defined sections along the microchannel and a two-step cascade reaction was conducted with full conversion after 30 seconds and high turnover frequencies (TOF* $\approx 10^5\ h^{-1}$*).*

"Vectorial catalysis", a defined multi-step reaction sequence, targets local multi-functionality integration and controlled active site access, enabled by spatial catalyst positioning combined with a transport gradient.[1] This concept stems from nature, as enzymes and their spatial assembly chemically and structurally control reaction environments over length scales to realize highly specific multi-step substrate transformations over intermediates to the final product at different active sites.[2] Mimicking this approach relies on distinct (as opposed to random) one-to-one interactions between reactants and specific sites, while drawing on advantages from continuous flow catalysis.[3] This is realized by localizing a succession of sites inside a channel and applying a gradient along the axial direction to drive the flux—a microfluidic reactor device.[1]

Such designed reaction sequestration requires precise multiscale reaction-specific nano- and micro-scale environment functionality organization, which is challenging for synthetic inorganic materials. Control elements include directed mass transport, induced orientation and alignment of reactants within confined spaces, and entatic reaction site states. These parameters rationalize using a modularly assembled compound class with synthetic control over void spaces, topologies, and physicochemical properties—metal–organic frameworks (MOFs).[4] The latter are formed by combining inorganic (metal–oxo) nodes and organic linkers, yielding coordination networks with permanent porosity.[5] Recent studies highlighted flexible catalyst system design benefiting from the molecular precision of MOF pore structures, their confined functionalized coordination space, and active species entrapment to precisely tailor reactivity.[6] However, MOF's potential in bio-mimicking vectorial catalysis remains unrealized, as most MOFs either focus on a one-step reaction or provide a "chemically-inert" host environment for the active species. Challenges include surface-selective MOF positioning and transport limitations due to unused inner pore volumes.[7]

This led us to develop a patterning technique to precisely position nanoscale MOFs on substrates to control their spatial orientation,[8] as well as improve substrate diffusion and increase reaction turnover frequencies (TOFs) by several orders of magnitude compared to their heterogeneous microcrystalline powder and quasi homogeneous colloidal MOF counterparts.[9]

Herein, we report MOF-based vectorial catalysis by integrating surface-anchored nanometer-sized MOFs (SA-NMOFs) as Lewis acidic catalysts into a microfluidic device. We provide a proof-of-principle model reactor setup to verify reaction sequestration with modular inorganic materials. We selected the two-step sequence hydrolysis of benzaldehyde dimethyl acetal (BADMA) to benzaldehyde (BA), followed by the Knoevenagel reaction of BA with malononitrile (MAN) to 2-benzylidene malononitrile (BACN). Established MOF catalysts were chosen,[10–12] which alluded that the MOFs' catalytic properties are compatible with the targeted reaction sequence. We employed benchmark polydimethylsiloxane (PDMS)-based microfluidic devices, providing a defined flow and programmable reaction space (Figure 1). Previous reports of MOF-integrated microfluidic appliances are limited and focus on MOF-based sensors or assays.[13] Instead we show controlled NMOF covalent anchoring at defined microscale channel sections, providing position-based sequential reactivity. We demonstrate the functionality of these SA-NMOF-decorated microfluidic devices, showing full conversion of BADMA to BACN in 30 s with high TOFs of $\approx 10^5\ h^{-1}$, orders of magnitude above bulk colloidal MOF catalysts.

We selected four MOF catalysts, namely UiO-66 ($Zr_6O_4(OH)_4(bdc)_6$, bdc = 1,4-benzene dicarboxylate), MIL-101, MIL-101-SO_3H, and MIL-101-NH_2. The latter consist of $Cr_3O(H_2O)(OH)^{6+}$ nodes and functionalized linkers (bdc-$SO_3Na)^{2-}$/(bdc-$SO_3H)^{2-}$, and bdc-$(NH_2)^{2-}$/(bdc-$NH_3)^-$(bdc-SO_3Na^{2-} = 2-sulfo-1,4-benzene dicarboxylate monosodium salt; bdc-NH_2^{2-} = 2-amino-1,4-benzene dicarboxylate). These were obtained as NMOFs following literature procedures with modifications,[14] and characterized by scanning electron microscopy (SEM), powder X-ray diffraction (PXRD),

[*] Dr. A. L. Semrau, P. M. Stanley, Dr. M. Cokoja, Prof. Dr. R. A. Fischer
Department of Chemistry
Inorganic and Metal-Organic Chemistry
Technical University of Munich
Lichtenbergstraße 4, 85787 Garching (Germany)
E-mail: roland.fischer@tum.de

D. Huber, Prof. Dr. M. Schuster
Department of Chemistry
Analytical Chemistry
Technical University of Munich
Lichtenbergstraße 4, 85787 Garching (Germany)

Dr. B. Albada, Prof. Dr. H. Zuilhof
Laboratory of Organic Chemistry
Wageningen University and Research
Stippeneng 4, 6708WE Wageningen (The Netherlands)

Prof. Dr. H. Zuilhof
School of Pharmaceutical Sciences and Technology
Tianjin University, 300072 Tianjin (China)

Prof. Dr. H. Zuilhof
Department of Chemical and Materials Engineering
Faculty of Engineering, King Abdulaziz University
21589 Jeddah (Saudi Arabia)

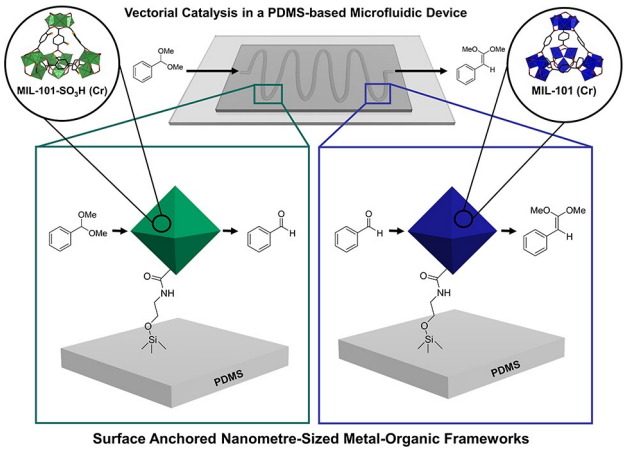

Figure 1. Microfluidic device concept. Two surface-anchored metal–organic frameworks (SA-NMOFs, green and blue octahedra) at predefined channel sections selectively catalyze one reaction sequence step from reactant (BADMA) to intermediate (BA) to product (BACN).

dynamic light scattering (DLS), and N_2 adsorption experiments (Figures S1–S3). The obtained PXRD patterns confirm crystalline, phase pure NMOF samples. Line broadening indicates reduced crystallite domain sizes, estimated by the Scherrer equation (Table S1).[15] The NMOF's primary particle sizes and the hydrodynamic radii were deduced from SEM and DLS measurements, respectively, confirming NMOF particle sizes between 21–157 nm.

Before microfluidic device integration, the NMOF series was evaluated in batch reactions for the hydrolysis of BADMA to BA and the subsequent reaction with MAN to BACN (Figure 2). An iterative optimization procedure to find compatible reaction conditions for each step, NMOF catalyst, and the PDMS-based microfluidic device was performed (Figures S4, S5). This yielded that i) acetonitrile (MeCN) or dioxane are compatible organic solvents, ii) H_2O ($\geq$125 equiv.) enhances the formation of BA and BACN, iii) more MAN equivalents enhances BACN formation, and iv) raising the temperature increases product formation, limited however by solvent evaporation. Within these boundaries, MIL-101-SO_3H and MIL-101-NH_2 were the most active catalysts for BADMA hydrolysis, while the Knoevenagel condensation was most effectively catalyzed by MIL-101. A crucial pre-requisite for an integrated cascade reaction system with all reactants simultaneously present is that each catalyst effectively catalyzes a single step and does not interfere with others. In other words, a set of orthogonal catalysts is required. Therefore, we verified whether this applies to our MOF-based Lewis acid catalysts by adding them subsequently in batch experiments and investigating the impact on product yields, i.e., BA, and BACN.

Specifically, when the catalysts were applied stepwise in the correct sequence (Figure 2b), BADMA reacts to BA within 6 h catalyzed by MIL-101-SO_3H. After removing MIL-101-SO_3H by filtration, 2 equiv. of MAN and 5 mg of MIL-101 were added and the final product BACN is formed.

However, if no catalyst is added (Figure 2c), or the catalyst order is reversed (Figures 2d, e), only 0 % (c), 8.9 % (d), or 17.5 % (e) BACN are obtained after 12 h. Consequently, the catalysts are sufficiently selective, do not interfere with the other reaction under these conditions, and conversion to the desired material requires specific catalyst–reagent matching.

Translating these results from batch reactions to a microfluidic continuous flow reactor required NMOF catalyst anchoring on the reactor's channel walls. As described

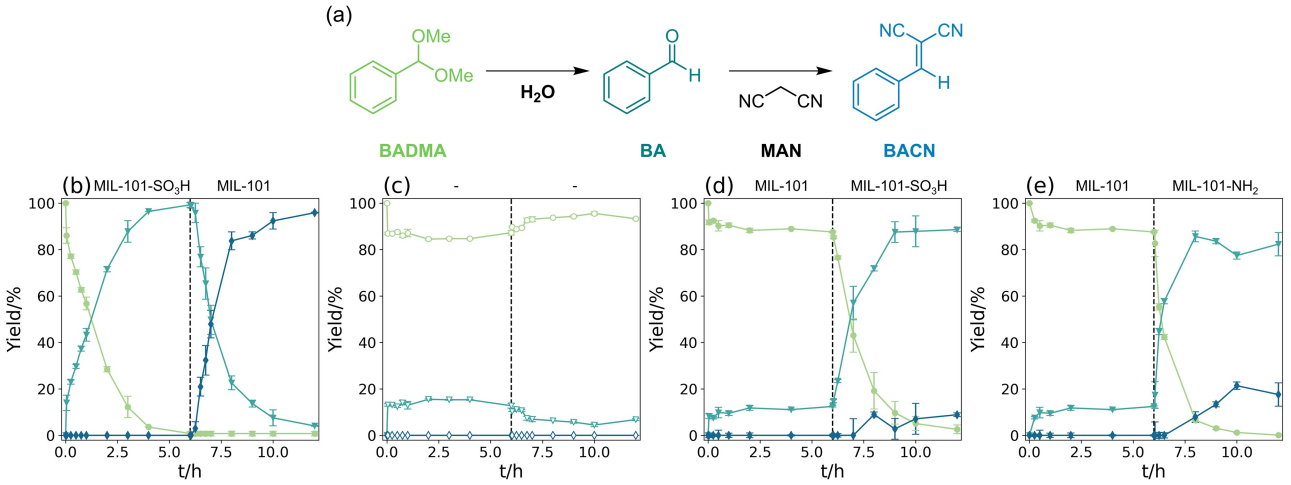

Figure 2. Prior to SA-NMOF microfluidic device integration, reaction conditions were screened in batch reactions using NMOF colloids: a) Targeted reaction sequence for vectorial catalysis: hydrolysis of benzaldehyde dimethyl acetal (BADMA) to benzaldehyde (BA), followed by the Knoevenagel condensation with malononitrile (MAN) to 2-benzylidene malononitrile (BACN). b)–e) Time-yield plots of BADMA (green, ●), BA (turquoise, ▼), and BACN (blue, ◆) for the reaction sequence in a batch reactor. The sequence was catalyzed by two different catalysts: catalyst **1** was applied for 6 h, removed and catalyst **2** was added with 2 equiv. of MAN. The applied catalysts are b) MIL-101-SO_3H/MIL-101; c) none/none; d) MIL-101/MIL-101-SO_3H and e) MIL-101/ MIL-101-NH_2. Reaction conditions: 0–6 h: 100 μM BADMA in 4:1.1 (v%) dioxane/water (5.1 mL) and 5 mg catalyst **1**, T=50 °C; 6–12 h: 100 μM BADMA, and 200 μM (2 equiv) MAN in 4:1.1 (v%) dioxane/water (5.1 mL) and 5 mg catalyst 2, T=50 °C.

previously,[8,9] we used amide bonds for covalent NMOF tethering to the substrate. These linkages were formed between dangling carboxylic acid functional groups at the NMOF particle's exterior surface and the amine-terminated functionalized substrate surfaces (i.e., PDMS, but also glass or silicon substrate surfaces were tested for comparison). These surfaces were then investigated by SEM (Figure S6) and inductively coupled plasma mass spectrometry (ICP-MS, Table S2). SEM reveals a relatively dense coating and even distribution of NMOF particles on the Si surface, which is especially pronounced for UiO-66 and MIL-101. The particle size distribution after particle anchoring decreased slightly while retaining a spherical particle shape. We assume that the electron beam damages the sample or that the anchoring process favours smaller particles over bigger ones. Nevertheless, the area-specific molar amount of active metal centres deposited at the surfaces (Si and PDMS) was determined at 0.66–5.31 nmol cm^{-2} via digestion of the SA-NMOF samples with H_2O_2/HNO_3 at 150 °C and measuring ICP-MS (Table S2). The obtained values are comparable with our previous data establishing the SA-NMOF methodology.[9]

Microfluidic device fabrication was achieved by PDMS-based molding and reactor sealing. First, SA-NMOF substrates (PDMS and glass) were fabricated via amide bond formation. Second, PDMS with an imprinted channel structure created with a mold is sealed to the NMOF functionalized substrate, forming the microfluidic device (Figures S7–S9). After assembly and based on the previously described characterization of our NMOFs and SA-NMOFs reference samples, we systematically investigated the microfluidic vectorial catalysis set-up and the impact on conversion, selectivity, and TOFs. A solution of BADMA and MAN in MeCN/H_2O or dioxane/H_2O was injected into the microfluidic device. By capillary forces, the solution traversed through the microreactor and eluted at the outlet, with a retention time of merely 30 s. Conversions were determined by analyzing eluting aliquots by GC, after diluting with MeCN or dioxane (Table 1). First, we used reactors loaded with one SA-NMOF catalyst, including a blank reactor (Table 1, entry 1), MIL-101-NH_2 (entry 2), MIL-101-SO_3H (entry 3), and MIL-101 (entry 4). The yields and conversions show zero conversion for the blank, and only the SA-NMOF loaded reactor with MIL-101 (entry 4) yielded a notable conversion of 15.5 % from BADMA to BA. The other two catalysts, i.e., MIL-101-NH_2 (entry 2) and MIL-101-SO_3H (entry 3), showed a higher conversion towards the intermediate BADMA, but the desired end-product BACN was not observed. However, we reached conversions of 85–90 % for BADMA and 72–82 % of the desired product BACN by applying the SA-NMOF catalysts in the optimal sequence, i.e., with MIL-101-NH_2 (entry 5) or MIL-101-SO_3H (entry 6) at position **1** of for BADMA hydrolysis, and with MIL-101 at position **2** for the Knoevenagel condensation. Note, the catalyst order is crucial as switching their positions led to 0 % product formation (entry 7). These results confirm our proof-of-concept with the first surface-bound NMOF-based microfluidic vectorial catalysis device. Further reaction parameter optimization including solvent, MAN equivalents, cycling experiments, and different substrate choices are provided in Table S3.

Table 1: Amounts of BADMA, BA, and BACN after vectorial catalysis (acetal hydrolysis followed by a Knoevenagel reaction) performed in PDMS-based microfluidic devices on SA-NMOF-functionalized PDMS substrates. The reactant concentrations were 125 μM BADMA and 1.25 mM (10 equiv.) MAN in 1:1 (v%) acetonitrile/water at room temperature with a retention time of 30 s.

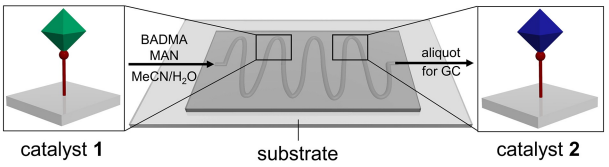

No	Catalyst **1**	Catalyst **2**	Amount [%] BADMA	BA	BACN
1	–	–	0.0	0.0	0.0
2	MIL-101-NH_2	MIL-101-NH_2	41.0	59.0	0.0
3	MIL-101-SO_3H	MIL-101-SO_3H	58.7	41.3	0.0
4	MIL-101	MIL-101	84.5	15.5	0.0
5	**MIL-101-NH_2**	**MIL-101**	**14.9**	**12.8**	**72.3**
6	**MIL-101-SO_3H**	**MIL-101**	**9.7**	**7.9**	**82.4**
7	MIL-101	MIL-101-SO_3H	74.5	25.5	0

(TOFs were calculated and the respective input data, calculation details, and applied assumptions are documented in the Supporting Information (chapter S1/Table S4). Here TOFs were exceptionally high and in the expected range based on SA-NMOF reference samples reported previously.[9] For the hydrolysis of BADMA, we found TOFs ≈1 000 000 h^{-1} for MIL-101-NH_2 as well as for MIL-101-SO_3H, and for the Knoevenagel reaction, we observed TOFs ≈400 000 h^{-1} for MIL-101. Relevant other publications on MOF-based tandem catalysts, which target full conversion of the reaction sequence by one bifunctional MOF catalyst, report significantly lower TOFs between 0.7–51 h^{-1}.[10,11,16] A comprehensive overview is shown in Tables 2 and S5.

Investigating the rate-limitation in the microfluidic devices with the random-walk equation shows that substrate diffusion to the SA-NMOFs is not the rate-determining step, but rather the diffusion into and within the SA-NMOFs (see Supporting Information, chapter S1). Therefore, the high TOFs can be explained by the small MOF particle sizes reducing diffusion limitations within the MOFs. Moreover, due to the surface anchoring of our catalysts, we prevent particle aggregation during catalysis, which would limit their catalytic activity.[9,17]

Realizing vectorial catalysis by integrating spatially localized and sequestrated catalytic sites in microfluidic devices is a visionary goal for bio-inspired catalysis research. We highlight the proof-of-principle nature of our two-step cascade study, chosen as an established and comparable model reaction to validate successful material assembly and controlled component hierarchy, enabling in-flow vectorial catalysis and validating the introduced concept based on SA-NMOF catalysts. The data implies the latter can be transferred to other reaction sequences. Further studies may use more sophisticated MOFs, integrate more catalyst sites

Table 2: TOF comparison from SA-NMOF based microfluidic devices presented in this study (+) with other literature values for bifunctional MOF tandem catalysts. If the TOF values were not given they were calculated with the data in these publications. A complete overview can be found in Table S5.

Catalyst	Solvent	T [°C]	t [h]	n_{cat} [mol %]	Amount [%] BA	BACN	TOF [h^{-1}] hydrolysis	TOF [h^{-1}] Knoevenagel condensation	Ref.
MIL-101-NH_2(Cr)	MeCN, H_2O	RT	0.008	0.008	12.8	72.3	1.13×10^6	–	+
MIL-101(Cr)	MeCN, H_2O	RT	0.008	0.02	12.8	72.3	–	4.05×10^5	+
PCN-124(Cu)	DMSO	50	12	1.0	0	100	16.8	16.8	[10]
MIL-101-NH_2(Al)	dioxane	90	3	43	6	94	0.76	0.74	[11]
Cr-MIL-101-AB-X	DMF	90	0.08	4.0	44	17	180	51	[16a]
Zn-MOF 1	DMF	80	0.5	1.0	16	10	52	20	[16b]
Cd-MOF 1	DMF	90	5	0.56	0	84	30	30	[16c]

and individual reaction steps, and utilize other microreactor fabrication materials such as cyclic olefin copolymers toward improved thermal stability and better solvent and reaction condition compatibility. Our results provide a perspective for microreactor device-integration with challenging reaction sequences using tailored MOF-based catalyst systems.

Acknowledgements

A.L.S. and P.M.S. acknowledge the Chemical Industry Fond for their PhD scholarships. This work was financially supported by Deutsche Forschungsgemeinschaft (DFG) project MOFMOX (FI 502/43-1) and DFG Priority Program 1928 "Coordination Networks: Building Blocks for Functional Systems". Open Access funding enabled and organized by Projekt DEAL.

Conflict of Interest

The authors declare no conflict of interest.

Data Availability Statement

The data that support the findings of this study are available in the Supporting Information of this article.

Keywords: Catalysis · Metal-organic frameworks · Microfluidic devices · Surface anchoring · Vectorial catalysis

[1] G. Centi, S. Perathoner, *Coord. Chem. Rev.* **2011**, *255*, 1480.
[2] a) D. M. Vriezema, P. M. L. Garcia, N. Sancho Oltra, N. S. Hatzakis, S. M. Kuiper, R. J. M. Nolte, A. E. Rowan, J. C. M. van Hest, *Angew. Chem. Int. Ed.* **2007**, *46*, 7378; *Angew. Chem.* **2007**, *119*, 7522; b) T. Vong, S. Schoffelen, S. F. M. van Dongen, T. A. van Beek, H. Zuilhof, J. C. M. van Hest, *Chem. Sci.* **2011**, *2*, 1278; c) M. H. Saier, *J. Bacteriol.* **2000**, *182*, 5029.
[3] a) I. Atodiresei, C. Vila, M. Rueping, *ACS Catal.* **2015**, *5*, 1972; b) R. Munirathinam, J. Huskens, W. Verboom, *Adv. Synth. Catal.* **2015**, *357*, 1093.
[4] a) R. Medishetty, J. K. Zaręba, D. Mayer, M. Samoć, R. A. Fischer, *Chem. Soc. Rev.* **2017**, *46*, 4976; b) A. Knebel, B. Geppert, K. Volgmann, D. I. Kolokolov, A. G. Stepanov, J. Twiefel, P. Heitjans, D. Volkmer, J. Caro, *Science* **2017**, *358*, 347; c) S. Okur, Z. Zhang, M. Sarheed, P. Nick, U. Lemmer, L. Heinke, *Sens. Actuators B* **2020**, *306*, 127502.
[5] S. R. Batten, N. R. Champness, X.-M. Chen, J. Garcia-Martinez, S. Kitagawa, L. Öhrström, M. O'Keeffe, M. Paik Suh, J. Reedijk, *Pure Appl. Chem.* **2013**, *85*, 1715.
[6] a) K. Hemmer, M. Cokoja, R. A. Fischer, *ChemCatChem* **2021**, *13*, 1683; b) P. M. Stanley, J. Haimerl, C. Thomas, A. Urstoeger, M. Schuster, N. B. Shustova, A. Casini, B. Rieger, J. Warnan, R. A. Fischer, *Angew. Chem. Int. Ed.* **2021**, *60*, 17854; *Angew. Chem.* **2021**, *133*, 17998.
[7] R. Freund, O. Zaremba, G. Arnauts, R. Ameloot, G. Skorupskii, M. Dincă, A. Bavykina, J. Gascon, A. Ejsmont, J. Goscianska et al., *Angew. Chem. Int. Ed.* **2021**, *60*, 23975; *Angew. Chem.* **2021**, *133*, 24174.
[8] A. L. Semrau, S. P. Pujari, P. M. Stanley, S. Wannapaiboon, B. Albada, H. Zuilhof, R. A. Fischer, *Chem. Mater.* **2020**, *32*, 9954.
[9] A. L. Semrau, P. M. Stanley, A. Urstoeger, M. Schuster, M. Cokoja, R. A. Fischer, *ACS Catal.* **2020**, *10*, 3203.
[10] J. Park, J.-R. Li, Y.-P. Chen, J. Yu, A. A. Yakovenko, Z. U. Wang, L.-B. Sun, P. B. Balbuena, H.-C. Zhou, *Chem. Commun.* **2012**, *48*, 9995.
[11] T. Toyao, M. Fujiwaki, Y. Horiuchi, M. Matsuoka, *RSC Adv.* **2013**, *3*, 21582.
[12] a) Y.-R. Lee, Y.-M. Chung, W.-S. Ahn, *RSC Adv.* **2014**, *4*, 23064; b) B. Li, Y. Zhang, D. Ma, L. Li, G. Li, G. Li, Z. Shi, S. Feng, *Chem. Commun.* **2012**, *48*, 6151.
[13] a) Y. H. Cheng, D. Barpaga, J. A. Soltis, V. Shutthanandan, R. Kargupta, K. S. Han, B. P. McGrail, R. K. Motkuri, S. Basuray, S. Chatterjee, *ACS Appl. Mater. Interfaces* **2020**, *12*, 10503; b) G. C. Ilacas, A. Basa, K. J. Nelms, J. D. Sosa, Y. Liu, F. A. Gomez, *Anal. Chim. Acta* **2019**, *1055*, 74.
[14] a) S. Wang, W. Morris, Y. Liu, C. M. McGuirk, Y. Zhou, J. T. Hupp, O. K. Farha, C. A. Mirkin, *Angew. Chem. Int. Ed.* **2015**, *54*, 14738; *Angew. Chem.* **2015**, *127*, 14951; b) P. Horcajada, C. Serre, D. Grosso, C. Boissière, S. Perruchas, C. Sanchez, G. Férey, *Adv. Mater.* **2009**, *21*, 1931; c) D. Jiang, L. L. Keenan, A. D. Burrows, K. J. Edler, *Chem. Commun.* **2012**, *48*, 12053; d) Y.-X. Zhou, Y.-Z. Chen, Y. Hu, G. Huang, S.-H. Yu, H.-L. Jiang, *Chem. Eur. J.* **2014**, *20*, 14976.
[15] U. Holzwarth, N. Gibson, *Nat. Nanotechnol.* **2011**, *6*, 534.
[16] a) H. Liu, F.-G. Xi, W. Sun, N.-N. Yang, E.-Q. Gao, *Inorg. Chem.* **2016**, *55*, 5753; b) A. Karmakar, M. M. A. Soliman, G. M. D. M. Rúbio, M. F. C. Guedes da Silva, A. J. L. Pombeiro, *Dalton Trans.* **2020**, *49*, 8075; c) S. Mistry, A. Sarkar, S. Natarajan, *Cryst. Growth Des.* **2019**, *19*, 747; d) A. Das, N. Anbu, M. S. A. Dhakshinamoorthy, S. Biswas, *Eur. J. Inorg. Chem.* **2020**, 2830.

[17] F. Maillard, S. Schreier, M. Hanzlik, E. R. Savinova, S. Weinkauf, U. Stimming, *Phys. Chem. Chem. Phys.* **2005**, *7*, 385.

Manuscript received: November 7, 2021
Accepted manuscript online: November 26, 2021
Version of record online: December 9, 2021